JUDD-OFELT THEORY: PRINCIPLES AND PRACTICES

BRIAN M. WALSH
NASA Langley Research Center
Hampton, VA 23681 USA
b.m.walsh@larc.nasa.gov,

1. Introduction

With few exceptions, no single idea is conceived without bringing together the work of previous ideas and forming a complete picture. So it was in August 1962 when there appeared in the literature, simultaneously and independently, two identical formulations of a theory. One by Brian R. Judd at the University of California at Berkeley and the other by a Ph.D. student, George S. Ofelt, at the Johns Hopkins University in Baltimore. Judd and Ofelt had never met personally, and were not aware of each other's interest in the intensities of rare earth ions in solids. While there are some differences in the two formulations, the approach and the assumptions used to arrive at the final result are remarkably similar. The titles of the two articles reflect a thought along similar lines. Judd referred to *Optical Absorption*, while Ofelt referred to *Crystal Spectra*, and each to Intensities of *Rare-Earth Ions*. The formulations as originally published by Judd and Ofelt came to be known as the Judd-Ofelt theory of the intensities of rare earth ions. Regarding these publications, the late Professor Brian G. Wybourne has said, "*I suggest that the coincidence of discovery was indicative that the time was right for the solution of the problem*" [1]. In the light of the advancement in the understanding of complex atomic spectra in the quarter century preceding the 1962 publications of Judd and Ofelt, this suggestion of Wybourne is based on very sound reasoning.

The rare earths comprise Y, Sc, La, Ce, Pr, Nd, Pm, Sm, Eu, Gd, Tb, Dy, Ho, Er, Tm, Yb and Lu. The last 15 make up the lanthanide series. Most of these elements were discovered over a period of time stretching from the late 18th century to the early 20th century. Promethium (Pm) was the last to be discovered in 1947 at Oak Ridge National Laboratory. So, with the exception of Promethium, all the rare earths were discovered in the span of a little more than a century. Part of the reason why they are called rare earths is two-fold. First, they are very difficult to chemically extract from the earth. Second, they do not exist in nature in high abundance. In the universe, the rare earths are approximately 10^6 times less abundant than the more common element silicon. In spite of their scarcity and difficulty in obtaining, the rare earths are highly valued for their unique properties, especially as optically active elements in their ionized state for lasers.

B. Di Bartolo and O. Forte (eds.), Advances in Spectroscopy for Lasers and Sensing, 403–433.

Even before the advent of lasers, the rare earths presented a *puzzle* in trying to understand their spectral properties in the context of the quantum theory that blossomed in 1920's and 1930's. In 1937 J.H. Van Vleck published an article titled *"The Puzzle of Rare-Earth Spectra in Solids"* [2]. He called it a puzzle because it was well known that rare earths exhibited sharp spectral lines, which would be expected if the transitions occurred between levels inside the 4*f* electronic shell. Such transitions were known to be *forbidden* by the Laporte selection rule, which says that states with even parity can be connected by electric dipole (E1) transitions only with states of odd parity, and odd states only with even ones. Another way of saying this is that the algebraic sum of the angular momenta of the electrons in the initial and final state must change by an odd integer. For transitions within the 4*f* shell, ED transitions are *forbidden*, but *allowed* for magnetic dipole (M1) or electric quadrupole (E2) radiation. The terms *forbidden* and *allowed* are not strictly accurate. The term *forbidden* means a transition may occur in principle, but with low probability. Given the relatively strong intensities and sharp spectral features of rare earth spectra, this picture presented a *puzzle* with the following possibilities:

1. 4*f* to 5d transitions.
2. Magnetic dipole or electric quadrupole radiation.
3. Electric dipole radiation.

The operators for E1, M1 and E2 transitions are shown in figure 1 along with their selection rules. It will be seen later that these selection rules will need to be modified under the Judd Ofelt theory.

$$\vec{P} = -e\sum_i \vec{r}_i \qquad \text{Electric dipole operator (E1)} \quad \text{(odd operator)}$$

$$\vec{M} = -\frac{e\hbar}{2mc}\sum_i \vec{\ell}_i + 2\vec{s}_i \qquad \text{Magnetic dipole operator (M1)} \quad \text{(even operator)}$$

$$\vec{Q} = \frac{1}{2}\sum_i (\vec{k}\cdot\vec{r}_i)\vec{r}_i \qquad \text{Quadrupole operator (E2)} \quad \text{(even operator)}$$

	S	L	J (No 0 ↔ 0)	Parity
Electric Dipole	$\Delta S = 0$	$\Delta L = 0, \pm 1$	$\Delta J = 0, \pm 1$	opposite
Magnetic dipole	$\Delta S = 0$	$\Delta L = 0$	$\Delta J = 0, \pm 1$	same
Electric quadrupole	$\Delta S = 0$	$\Delta L = 0, \pm 1, \pm 2$	$\Delta J = 0, \pm 1, \pm 2$	same

Figure 1. Multipole operators and selection rules.

The solution to this *puzzle* was proposed by Van Vleck [2] in 1937 and further resolved by Broer, *et al*. [3] in 1945. The first possibility would be indicative of broad spectral lines in contrast to the sharp lines that were observed. Magnetic dipole radiation could account for some transitions, but not all transitions, and represents a special case. Quadrupole radiation could

account for all the transitions, but was too weak to account for the observed intensities. Only ED radiation was a reasonable solution, but it is forbidden by the Laporte selection rule. The solution considered a distortion of the electronic motion by crystalline fields in solids, so that the selection rules for free atoms no longer applied.

Not all crystalline fields are capable of producing this effect. The crystal field must be noncentrosymmetric, that is, lacking a center of symmetry at the equilibrium position, otherwise the wavefunctions would retain an even or odd parity with regards to reflection about the origin. If the wavefunctions retained their even or odd parity, then Laporte's rule (even states can connect to odd states and odd to even) would remain rigorous, and electric dipole radiation would be strictly forbidden. In other words, In order to have a change of parity, the odd-order terms of the crystalline field, expressed as a power series in the displacement from equilibrium, must be present. These terms vanish for a central field, and no change of parity can occur. The odd-order terms of a noncentral crystalline field can force a coupling between odd and even states, resulting in mixed parity states that mitigates Laporte's rule.

It would take another 25 years after Van Vleck's paper before the appearance of the papers by Judd and Ofelt. What is the reason for the quarter century gap? The main reason is that the techniques of group theory were not applied to lanthanides until 1949 and, even then, it took some years for these ideas to be absorbed, incorporated and accepted. The seminal papers by Guilio Racah in the 1940's would revolutionize the entire subject of complex spectra. In a series of papers [4,5,6], culminating in his 1949 paper [7] regarding $4f$ electrons, he created a powerful set of tools that made possible many complex spectroscopic calculations. The work of Condon and Shortly [8] in *"The Theory of Atomic Spectra"* published in 1935 is a classic and seminal work in itself, but the tools are much more cumbersome than the newer group theory. The ideas of Racah took some time to root and proved to be a key ingredient in the solution to a problem regarding the calculation of forced electric dipole transitions. The concept of representing operators as irreducible tensors and their subsequent manipulation would play a pivotal role in the solution of the problem. Another reason for the delay between Van Vleck's paper and those of Judd and Ofelt concerns the dawn of computers. The computer made possible the tabulation of all angular momentum coupling coefficients [9]. This did not occur until 1959, but by then the stage was set for a revolution in understanding the complex spectra of lanthanide ions. The decade of the 1960's can be viewed as a revolution in spectroscopic research on rare earth ions. This decade saw the invention of the laser go from a device in search of an application to applications in search of laser devices. The theory of Judd and Ofelt remains in history at the forefront of this revolution.

2. Ions in Solids

An ion in a solid can be considered as an impurity embedded in a solid host material, usually in small quantities. These impurities replace the host ions substitutionally and form optically active centers which exhibit luminescence when excited by an appropriate excitation source. When speaking of solids in general, a glass or crystal is implied. The former is amorphous over a long range, but may contain local order. The later has definite long-range order in a lattice structure. Both glasses and crystals are insulators, distinguishing them from semiconductors, and have bandgaps greater than 5 eV, which is about the wavelength of photons in the deep

UV. The host material plays a fundamental role in determining the nature of the observed spectra of the optically active impurity ions. This is known as Ligand field theory in general and crystal field theory in the case of an ordered periodic lattice.

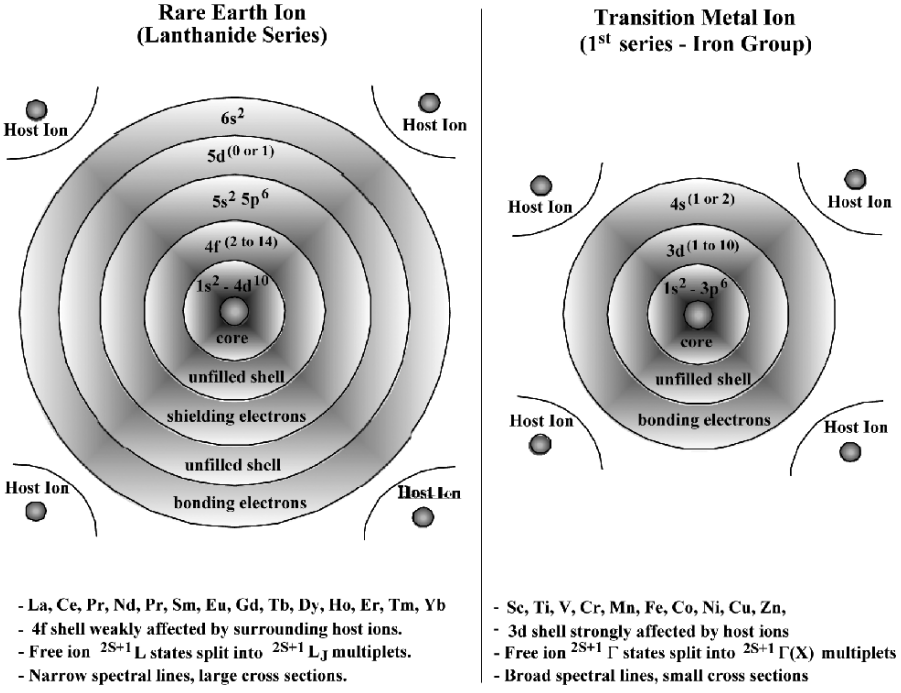

Figure 2. Rare Earth and Transition metal ion atomic structure.

Now, the impurity ions, usually called dopant ions, are the optically active centers. The host is generally transparent. The impurities, dopant ions, are transition metal or lanthanide series ions characterized by unfilled shells in the interior of the ion. The atomic structure of rare earth ions in the lanthanide series and transition metal ions of the iron group are shown in figure 2. These representations are not drawn to scale and are shown simply to give an overall visual representation of their structure. All lanthanide ions are characterized by a Xe core, an unfilled $4f$ shell, and some outer shells that screen the $4f$ shell from outside perturbing influences. This screening effect protects the optically active electrons to some extent from the influence of the crystal field, giving the lanthanides their characteristic sharp and well defined spectral features. In other words they are very similar to free ion spectra. This is in contrast to transition metals where the unfilled 3d shell is not as well screened due to only a single outer shell. The

transition metals are characterized by broad, undefined features, although some sharp lines are observed. The R_1 and R_2 lines of $Cr:Al_2O_3$, ruby, for example, are sharp lines. Transition metals are, therefore, strongly coupled to the lattice and susceptible to the vibrational motions of the host lattice ions. The energy levels for transition metals are more vibrational-electronic, or vibronic, whereas the lanthanides are more electronic. These transitions occur within the bandgap of the material and have a range out to about 5 eV. In terms of wavelength, transitions are observed from about 0.2 to 5.0 micrometers.

As just stated, the crystal field plays an important role in influencing the features of optical spectra. It also plays an obvious role in the Stark effect regarding the splitting of energy levels of ions in solids. It is the influence it has on the ionic states regarding selection rules that makes such transitions possible, as will be discussed. The ligand, or crystalline field is totally external to the optically active dopant ion and has the symmetry determined by the chemical composition of the host. In an ionic crystal, the optically active dopant ions feel the influence of electrons, belonging to crystal host ions, as a repulsion, and of the nuclei, belonging to the crystal host, as an attraction. The accumulation of these influences can be considered as a net electric field, known as the crystalline field. In this context, lanthanide ions exist in the weak field scheme, while transition metals of the iron group such as chromium, Cr, exist in the medium field scheme. In the former the crystal field is small in comparison to spin-orbit interactions, whereas in the later the crystal field is large compared to spin-orbit interactions. The crystal field plays a fundamental role in making many laser transitions possible.

An obvious question is to what extent the crystal field splits the energy levels and how many levels are obtained for a given crystal field? To begin to answer this question, consider the free ion Hamiltonian,

$$H_F = -\frac{\mathrm{h}^2}{2m}\sum_{i=1}^{N}\nabla_i^2 - \sum_{i=1}^{N}\frac{Ze^2}{r_i} + \sum_{i<j}^{N}\frac{Ze^2}{r_{ij}} + \sum_{i=1}^{N}\xi(r_i)(\mathbf{s}_i \cdot \mathbf{l}_i) \tag{1}$$

The first term is the sum of the kinetic energies of all the electrons of a 4f ion, the second term is the potential energy of all the electrons in the field of the nucleus. The third term is the repulsive Coulomb potential of the interactions between pairs of electrons, and the last term is the spin-orbit interaction, which accounts for coupling between the spin angular momentum and the orbital angular momentum. In terms of the central field approximation, each electron can be considered to be moving independently in the field of the nucleus and a spherically averaged potential of all the other electrons. The Coulomb interaction produces different SL terms with different energies, but is independent of the total angular momentum J of the electrons. The spin-orbit interaction allows coupling between states of different SL and thus is dependent on the total angular momentum. In the language of quantum mechanics, the spin orbit operator does not commute with $\mathbf{L}^2$ and $\mathbf{S}^2$, but it does commute with $\mathbf{J}^2$ and J_z. In simple terms this means that the Coulomb interaction removes degeneracy in S and L, while the spin orbit interaction removes degeneracy in J. The M_J degeneracy remains. This is only removed by the crystal field. The atomic interactions and energy level splittings are depicted in figure 3.

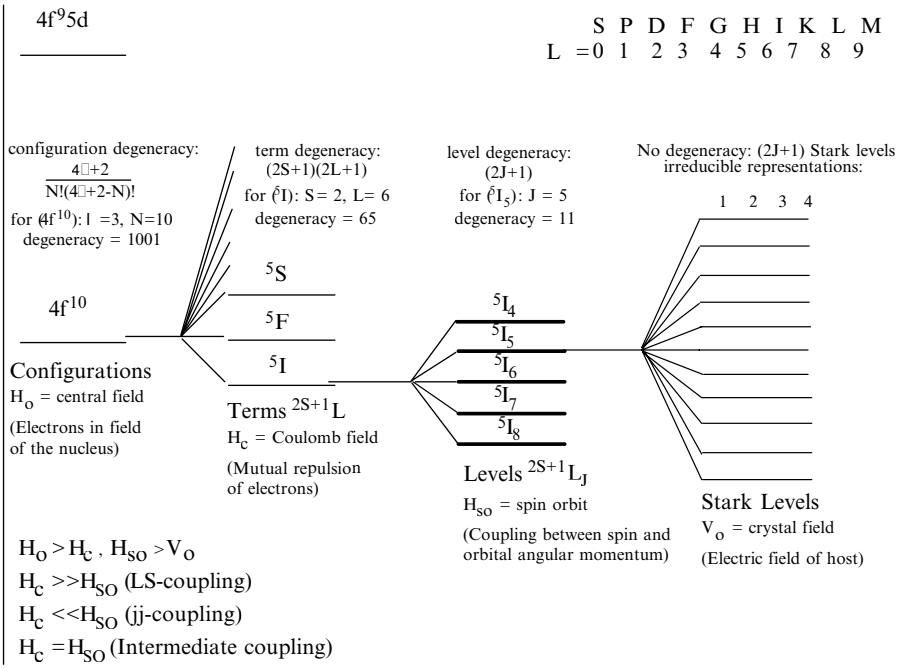

Figure 3. Rare earth and transition metal ion atomic structure.

So, in the free atom there is a spherical symmetry and each level is reduced to 2J+1 degeneracy. When the ion is placed in a crystal environment the spherical symmetry is destroyed and each level splits under the influence of the crystal field. In fact, the spherical symmetry is reduced to the point symmetry at the ion site. The degree to which the 2J+1 degeneracy is removed will depend on the point symmetry surrounding the ion. This aspect will become clear shortly. The perturbed free ion Hamiltonian for an ion in a crystal is written as,

$$H = H_F + V_{CF} \tag{2}$$

where V_{CF}, the perturbation Hamiltonian, is due to the potential provided by the crystal environment around the ion. Since the eigenfunctions of the free Hamiltonian possess complete spherical symmetry and are expressible in terms of spherical harmonics, it is natural to expand V in terms of spherical harmonics,

$$V_{CF} = \sum_{kq} A_{kq} \sum_{i} r_i^k Y_{kq}(\vartheta_i, \varphi_i) \tag{3}$$

where the summation over i involves all electrons of the ion of interest. The A_{kq} are structural parameters in the static crystal field expansion. They depend only on the crystal host and can be calculated in a point charge lattice sum using crystallographic data and charges of the host lattice. The point charge model assumes that the charges of the host lattice are all point charges. The A_{kq} are then given by,

$$A_{kq} = -q_e \sum_{i} \frac{Z_i Y_{kq}(\vartheta_i, \varphi_i)}{R_i^{k+1}} \tag{4}$$

where q_e is the electronic charge, Z_i is the size of the charge at position R_i corresponding to the surrounding atoms composing the crystal. In the calculation of matrix elements, $\langle \alpha | V | \beta \rangle$, there results matrix elements of the form $\langle r^k \rangle = \langle n\ell | r^k | n\ell \rangle$, that represent the average value of r^k. This leads to terms of the form,

$$B_{kq} = A_{kq} \left\langle r^k \right\rangle \tag{5}$$

These terms enter prominently in the calculation of energy levels. They are generally determined empirically from experimental data, that is, by fitting the measured energy levels to the theory by a least squares iterative fitting procedure. Once the point symmetry and the appropriate form of the crystal field are known, it is possible to construct the crystal field energy matrix. This matrix is then diagonalized using an estimated set of B_{kq} starting parameters. The resulting set of theoretical energy levels are compared to the set of experimental levels and, by an iterative fitting procedure, the B_{kq} parameters are adjusted to obtain the best overall fit to experiment. The thirty-two crystallographic point groups can be divided into four general symmetry classes as follows [10]:

1. Cubic: O_h , O , T_d ,T_h , T
2. Hexagonal: D_{6h} , D_6 ,C_{6v} , C_{6h} , C_6 , D_{3h} , C_{3h} , D_{3d} , D_3 , C_{3v} , S_6 , C_3
3. Tetragonal: D_{4h} , D_4 , C_{4v} , C_4 , D_{2d} , S_4
4. Lower symmetry: D_{2h} , D_2 , C_{2v} , C_{2h} , C_2 , C_s , S_2 , C_1

Now, if the initial and final states have the same parity, then k must be even. If the initial and final states have opposite parity then k must be odd. Otherwise, the matrix elements of V_{CF} are zero. So, if a matrix element of an operator of rank k connects angular momenta ℓ and ℓ' then the triangle condition, $\ell + \ell' \geq k \geq |\ell - \ell'|$, must hold. For 4f electrons, $\ell = \ell' = 3$, and k must, therefore, be even for transitions within the f^n configuration, and is limited to values k = 0, 2, 4, 6. However, if states of the f^n configuration are coupled to states of opposite parity in higher lying configurations, such as $4f^{(n-1)}$ 5d, then $\ell = 3$ and $\ell' = 2$. In this case k is odd and

is limited to values k = 1, 3, 5. These odd-order terms play a key role in the Judd-Ofelt theory for forced electric dipole transitions in lanthanide and actinide ions in solids. The values for k and q are also limited by the point symmetry of the ion. That is, the number of nonzero terms is dependent on the point symmetry. This arises from the fact that the Hamiltonian must be invariant under operations of the point symmetry group. Thus, the crystal field must also exhibit the same symmetry as the point symmetry of the ion, since it is part of the total Hamiltonian. Equating the crystal field expansion with the expansion that has been transformed through operations of the point symmetry group gives the allowed crystal field parameters for a particular ionic point symmetry. Thus, the spherical symmetry of an ion in a crystal is reduced to the point symmetry at the site of the ion. It is noted that terms with k = 0 and q = 0 are spherically symmetric and affect all energy levels in the same way, resulting in only a uniform shift of all levels in the configuration. The cases where q = 1 and q = 5 occur only when there is no symmetry, as for C_1. In general, the values of q are restricted to $q \leq k$, but the point symmetry introduces further restrictions, and this determines the allowed values of q.

It can be shown that knowledge of the symmetry class at the site of the ion can be used to predict the number of levels a given J state splits into. The number of levels given J state splits into for a given point symmetry is presented in table I [10]. Alternatively, rare-earth ions can be used to probe the crystal symmetry if the number of levels of the ion can be determined.

TABLE I. Number of levels for integral J

J =	0	1	2	3	4	5	6	7	8
Cubic	1	1	2	3	4	4	6	6	7
Hexagonal	1	2	3	5	6	7	9	10	11
Tetragonal	1	2	4	5	7	8	10	11	13
Lower symmetry	1	3	5	7	9	11	13	15	17

As has already been stated, the positions of the levels arise from a combination of the Coulomb, spin-orbit, and crystal field interactions. The electrostatic interaction leads to ^{2S+1}L splitting on the order of 10^4 cm^{-1}. The spin-orbit interaction splits the levels further into $^{2S+1}L_J$, separating the J states by 10^3 cm^{-1}. Finally, the crystal field removes or partially removes the degeneracy in J yielding an energy level separation on the order of 10^2 cm^{-1}. The extent to which the Stark split sublevels spread is dependent on the strength of the crystal field. The larger the crystal field, the larger will be the spread of the J sublevels.

Consider the lanthanide ions as an example. The lanthanide ions are characterized by a shielded 4*f* shell where the atomic like transitions take place. The 4*f* states all have the same parity, that is $(-1)^{\Sigma \ell_i}$, where $\ell = 3$ for lanthanides. The question then arises, where do opposite parity states that are *mixed* in come from? They come from shells above the 4*f* shell, such as 5d. The d electrons have $\ell = 2$ and so have opposite parity to f electrons. The wavefunctions for some 1s to 6*f* states are pictured in figure 4. This figure provides a nice pictorial representation of the parity of the wavefunctions for various orbitals. For instance, the *f* orbitals clearly have

odd parity since there is a change in sign on reflection about the origin. Similarly, the d orbitals have even parity as the sign is preserved on reflection about the origin.

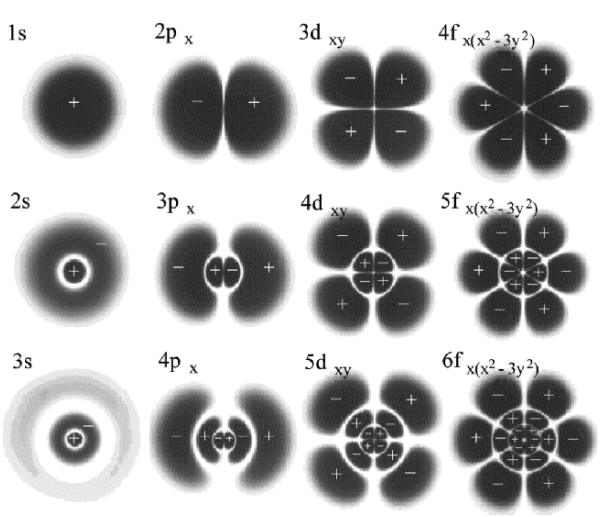

Figure 4. Wavefunctions of some s, p, d and f orbitals.

A typical wavefunction for an ion in a crystal can be expressed as a linear combination of states in the free ion, which are composed of sums of both even and odd parity wavefunctions, and form a complete orthonormal set of basis functions. This allows for mixed parity states via the odd-order terms of the crystal field mentioned earlier. As a result, electric dipole transitions can be forced through parity mixing and result from the perturbation caused by the odd-order terms of the crystal field. Nature finds a way around Laporte's rule in this way. Since these transitions come about as a result of a perturbation, they are orders of magnitude smaller than in free ions, but strong enough to produce a plethora of transitions from which many lasers can be realized. This, in itself, is a remarkable circumstance of opportunity. The theory that predicts the intensities of such transitions, the Judd-Ofelt theory, is discussed in the next section.

3. Judd-Ofelt Theory: Principles

The Judd-Ofelt theory [11,12] is based on the static, free-ion and single configuration approximations. In the static model, the central ion is affected by the surrounding host ions via a static electric field, referred to as the ligand or crystal field. In the free-ion model, the host environment produces the static crystal field, and is treated as a perturbation on the free-ion Hamiltonian. In the single configuration model, the interaction of electrons between configurations

is neglected. Simply stated, the Judd-Ofelt theory describes the intensities of lanthanide and actinide transitions in solids and solutions. The utility of the Judd-Ofelt theory is that it provides a theoretical expression for the line strength, given by,

$$S_{ED}(J;J') = \sum_{\lambda=2,4,6} \Omega_\lambda \left| \left\langle f^n[SL]J \left\| \mathbf{U}^{(\lambda)} \right\| f^n[S'L']J' \right\rangle \right|^2 \tag{6}$$

where Ω_λ are the *Judd-Ofelt parameters*. The terms in brackets are doubly reduced matrix elements for intermediate coupling. Intermediate coupling refers to a situation where the mutual repulsion interaction between 4f electrons is of the same order of magnitude as the spin-orbit coupling. This effect can be incorporated by expanding the wavefunctions of the 4*f* states in a linear combination of *Russel-Saunders*, or LS-coupled states. The coupling coefficients are found by diagonalizing the combined electrostatic, spin orbit and configuration interaction energy matrices to obtain the full intermediate coupled wavefunctions, $|f^n[\mathrm{SL}]\mathrm{J}\rangle$. A substantial portion of the book *"Spectroscopic coefficients of the* p^n, d^n, and f^n *configurations"* by Nielson and Koster [13] is devoted to tabulating matrix elements in LS coupling. Further efforts must be devoted to converting these wavefunctions to the intermediate coupling case applicable to lanthanide ions. Fortunately, many references tabulate intermediate coupled matrix elements based on Nielson and Koster's work. Because the electric dipole transitions arise from a small crystal field perturbation, the matrix elements are not highly dependent on the host material.

These matrix elements are integrals of the dipole operator between the upper and lower wave functions of the transition, where the integration takes place over the volume of the atom. The $\mathrm{U}^{(\lambda)}$ in Eq. (6) are the irreducible tensor forms of the dipole operator. Basically, during the transition the atom can be considered an electric dipole oscillating at some frequency whose amplitude is proportional to the value of this matrix element. It is the interaction of this dipole moment with the electric field of the electromagnetic wave that induces the transition. It is analogous to a classical oscillating dipole driven by an external electric field. Quantum mechanically, the situation is more complicated because the parity between the upper and lower electronic states must be considered. In quantum mechanics, electric dipole transitions between electronic states of the same parity are forbidden. This is basically a result of the fact that the expectation value of the position operator, **r**, is odd under reflection, and vanishes for definite parity. The electronic states have wavefunctions described by spherical harmonics, and as such, have the parity of the angular quantum number ℓ. Considering an electronic shell as a whole, the total parity for an n electron system is $\wp = (-1)^{\ell_1 + \ell_2 + \ldots + \ell_n}$, therefore, an even number of electrons has parity of $\wp = 1$ and an odd number of electrons has parity $\wp = -1$. This means that, regardless of the number of electrons, all states in the 4*f* shell always has definite parity. In free ions, this means that ED transitions within the 4*f* shell of lanthanide ions are forbidden. However, electric dipole transitions can be forced if opposite parity states from higher lying configurations outside the 4*f* shell are mixed into the upper state. This is possible when the atom is placed in a noncentrosymmetric perturbing field such as the crystal field of a lattice in which the atom is embedded. This does not happen in a central field because the Hamiltonian is invariant under coordinate inversion, and the states retain definite parity. The odd-order parts of

the crystal field, expanded in a series of spherical harmonics, perturb the system and produce mixed parity states between which electric dipole transitions are allowed. This is, in fact, the starting point from which the Judd Ofelt theory is based.

If the crystal field is taken as a first-order perturbation, then the initial and final mixed parity states, $\langle\psi_a|$ and $|\psi_b\rangle$, can be expanded as:

$$\langle\psi_a| = \langle\varphi_a| + \sum_\beta \frac{\langle\varphi_a|V|\varphi_\beta\rangle}{E_a - E_\beta}\langle\varphi_\beta| \tag{7}$$

$$|\psi_b\rangle = |\varphi_b\rangle + \sum_\beta \frac{\langle\varphi_\beta|V|\varphi_b\rangle}{E_b - E_\beta}|\varphi_\beta\rangle \tag{8}$$

where $\langle\varphi_a|$ and $|\varphi_b\rangle$ are the initial and final states of single parity. The φ_β are states of higher energy, opposite parity configurations. The electric dipole matrix elements, $D = \langle\psi_a|\ \mathbf{P}\ |\psi_b\rangle$, can now be found, where **P** represents the electric dipole (ED) operator given by,

$$\mathbf{P} = -e\sum_i \mathbf{r}_i \tag{9}$$

Combining the terms from Eq. (7) and Eq. (8) about the electric dipole operator, it is clear that $\langle\varphi_a|\ \mathbf{P}\ |\varphi_b\rangle = 0$ and $\langle\varphi_\beta|\ \mathbf{P}\ |\varphi_\beta\rangle = 0$ since dipole transitions are forbidden between states of the same parity. The expression for the electric dipole matrix element, *D*, reduces to,

$$D = \langle\psi_a|\mathbf{P}|\psi_b\rangle = \sum_\beta \left\{ \frac{\langle\varphi_a|V|\varphi_\beta\rangle\langle\varphi_\beta|\mathbf{P}|\varphi_b\rangle}{E_a - E_\beta} + \frac{\langle\varphi_a|\mathbf{P}|\varphi_\beta\rangle\langle\varphi_\beta|V|\varphi_b\rangle}{E_b - E_\beta} \right\} \tag{10}$$

It is useful to introduce tensor forms of the crystal field and ED operator. Tensor forms are useful because they can easily be combined into a single effective tensor operator. The crystal field and ED operators, Eq. (3) and Eq. (9), respectively, have the tensor operator forms:

$$\mathbf{D}_q^{(1)} = -e\sum_i r_i \left[\mathbf{C}_q^{(1)}\right]_i \tag{11}$$

$$\mathbf{D}_p^{(t)} = \sum_{tp} A_{tp} \sum_i r_i^t \left[\mathbf{C}_p^{(t)}\right]_i \tag{12}$$

The $\mathbf{C}_q^{(k)}$ are tensor operators that transform like spherical harmonics,

$$\mathbf{C}_q^{(k)} = \left(\frac{4\pi}{2k+1}\right)^{1/2} Y_{kq} \tag{13}$$

For instance, the position operator, **r**, is a tensor of rank one and is defined as $\mathbf{r} = r\mathbf{C}^{(1)}$. This gives the spherical harmonics as $Y_{10} = -(3/4\pi)^{1/2} \cos\theta$ and $Y_{1,\pm1} = \mp (3/8\,\pi)^{1/2} \sin\theta\, e^{\pm i\varphi}$ for k = 1, q = 0, ±1. The resulting components are then written as $z = r\cos\theta$ and $\mp (x \pm iy)/\sqrt{2}$, where $x = r\sin\theta\cos\theta$ and $y = r\sin\theta\ \sin\theta$, such that $r = (x^2 + y^2 + z^2)^{1/2}$.

A couple of assumptions can now be made to simplify the problem. The first is to assume an average energy for the excited configurations above the $4f^n$. The second is to assume that the difference of the average energies, $\Delta E(4f\text{-}5d)$, is the same as the difference between the average energy of the $4f^{(n-1)}5d$ and the energy of the initial and final state of the $4f^n$ configuration. These assumptions can be summarized as follows:

1. The states of $|\varphi_\beta\rangle$ are completely degenerate in J.
2. The energy denominators in Eq. (10) are equal ($E_a - E_\beta = E_b - E_\beta$).

The relative positions of the $4f^n$ and $4f^{(n-1)}5d$ configurations are shown in figure 5 for comparison. So, for most of the rare earth ions these assumptions are only moderately met, but offer a great simplification. Otherwise, the many fold sum of perturbation expansions would not be suitable for numerical applications. The advantage of these assumptions allows the energy denominators to be removed from the summations and closure, $|\varphi_\beta\rangle\langle\varphi_\beta| = 1$, to be used. What does it mean to use closure? From basic quantum mechanics, any wavefunction can be expanded in a suitable set of orthonormal basis functions and written as $|\psi\rangle = \Sigma_n\, a_n|\varphi_n\rangle$, such that $\langle\varphi_m|\varphi_n\rangle = \delta_{mn}$ and, therefore, $a_n = \langle\varphi_m|\psi\rangle$. Hence, it follows that $|\psi\rangle = \Sigma_n\, a_n|\varphi_n\rangle\langle\varphi_n|\psi\rangle$, and so, $|\varphi_\beta\rangle\langle\varphi_\beta| = 1$. This is closure and the meaning, as it applies here, is that the states of the excited configuration form a complete orthonormal set of wavefunctions. Once closure is invoked, the angular parts of the crystal field, $\mathbf{C}^{(1)}_q = \langle\ell\|\mathbf{C}^{(1)}\|\ell'\rangle\, \mathbf{U}^{(1)}_q$ and electric dipole operator, $\mathbf{C}^{(t)}_p = \langle\ell\|\mathbf{C}^{(t)}\|\ell'\rangle\, \mathbf{U}^{(\lambda)}_Q$, can be combined into an effective tensor operator, that is,

$$\mathbf{U}^{(1)}_q \mathbf{U}^{(t)}_p = \sum_{\lambda Q} (-1)^{1+t+\lambda+Q} (2\lambda+1) \begin{Bmatrix} 1 & t & \lambda \\ l & l & l' \end{Bmatrix} \begin{pmatrix} 1 & t & \lambda \\ q & p & Q \end{pmatrix} \mathbf{U}^{(\lambda)}_Q \tag{14}$$

where Q = – (q + p), and λ = 1 + t. The 3j symbol ( ) is related to the coupling probability for two angular momenta. The 6j symbol { } is related to the coupling probability for 3 angular momenta. These are known as Wigner symbols. The Wigner 3j and 6j symbols are related to Clebsch-Gordon coefficients. In addition, the effective tensor operator, can be further simplified by utilizing the Wigner-Eckart theorem,

$$\left\langle JM \left| \mathbf{U}^{(\lambda)}_Q \right| J'M' \right\rangle = (-1)^{J-M} \begin{pmatrix} J & \lambda & J' \\ -M & Q & M' \end{pmatrix} \left\langle J \left\| \mathbf{U}^{(\lambda)} \right\| J' \right\rangle \tag{15}$$

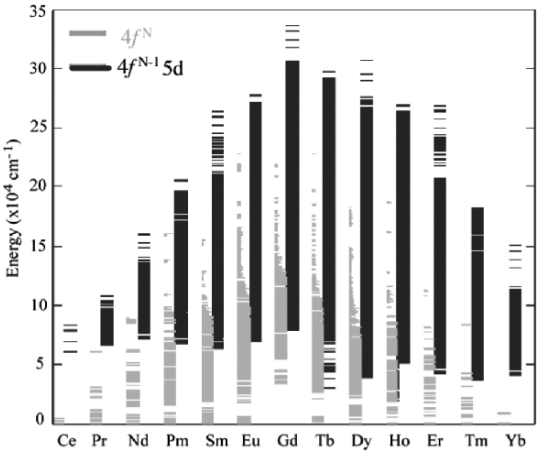

Figure 5. Energy levels of the $4f^n$ and $4f^{(n-1)}5d$ lanthanides.

The Wigner-Eckart theorem is a remarkable equation because it separates the geometry from the physics. The geometry of the angular momentum transformations are in the 3j symbol, while the physics of the dynamics is in the reduced matrix element of $\mathbf{U}^{(\lambda)}$. The full solution is,

$$D = -e\sum_{tp}\sum_{\lambda Q}(-1)^{J-M-Q}(2\lambda+1)A_{tp}Y(t,\lambda)\begin{pmatrix}1 & t & \lambda\\ q & p & Q\end{pmatrix}\begin{pmatrix}J & \lambda & J'\\ -M & Q & M'\end{pmatrix}\left\langle \varphi_a \left\| \mathbf{U}^{(\lambda)} \right\| \varphi_b \right\rangle \qquad (16)$$

where, $Y(t, \lambda)$ is given by,

$$Y(t,\lambda) = 2\sum_{nl}\frac{\langle 4f|r|nl\rangle\langle nl|r^t|4f\rangle}{\Delta E_{nl}}\left\langle f\left\|\mathbf{C}^{(1)}\right\|l\right\rangle\left\langle l\left\|\mathbf{C}^{(t)}\right\|f\right\rangle\begin{Bmatrix}1 & t & \lambda\\ l & l & l'\end{Bmatrix} \qquad (17)$$

and A_{tp} are parameters of the static crystal field expansion, Eq. (4), with t → k and p → q. This is the full solution of the Judd-Ofelt theory. This form can be used to find electric dipole matrix elements between mixed parity states for individual Stark level to Stark level transitions [14]. In the above equation for $Y(t,\lambda)$, $\Delta E_{n\ell}$ is the energy difference between the $4f$ and opposite parity, $n\ell$ configuration. The first two terms are the interconfiguration radial integrals:

$$\langle 4f|r|nl\rangle = \int_0^\infty R(4f)rR(nl) \qquad (18)$$

$$\langle nl|r^t|4f\rangle = \int_0^\infty R(nl)r^tR(4f) \qquad (19)$$

while the second two terms are reduced matrix elements of the tensor operator $\mathbf{C}_q^{(k)}$, which represents the angular part of the crystal field, and can be calculated from the angular momentum quantum numbers of the configurations according to the equations:

$$\left\langle f \left\| \mathbf{C}^{(1)} \right\| \mathrm{l} \right\rangle = (-1)^{\mathrm{l}} \left(2\mathrm{l}+1\right)^{1/2} \left(2f+1\right)^{1/2} \begin{pmatrix} f & 1 & \mathrm{l} \\ 0 & 0 & 0 \end{pmatrix} \tag{20}$$

$$\left\langle \ell \left\| \mathbf{C}^{(t)} \right\| f \right\rangle = (-1)^{f} \left(2\mathrm{l}+1\right)^{1/2} \left(2f+1\right)^{1/2} \begin{pmatrix} \mathrm{l} & t & f \\ 0 & 0 & 0 \end{pmatrix} \tag{21}$$

Finally, the last term is a 6j symbol, associated with transformations between angular momentum coupling schemes. In this case, it arises through the coupling of the electric dipole and crystal field operators. It is noted that t takes on only odd values in the summations above, since only the odd-order terms in the multipole expansion of the crystal field contribute to parity mixing. The even-order terms are only responsible for shifting and splitting of the energy levels. It is possible to say something about the selection rules in the Judd-Ofelt theory at this point. The selection rules can be derived from the properties of the 3j and 6j symbols, illustrated in figure 6, and are an extension from what was shown in figure 1.

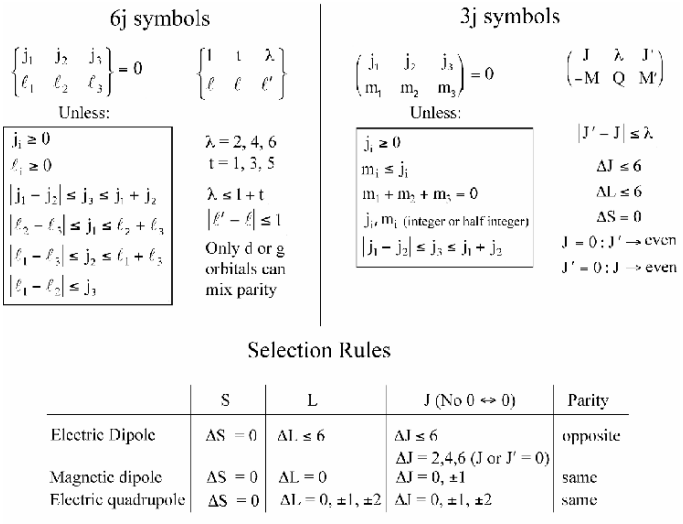

Figure 6. Selection Rules in the Judd-Ofelt Theory.

In the form of Eq. (16) the theory is suitable for calculating transitions between individual Stark levels. However, Judd and Ofelt were interested in ions in solution where individual Stark transitions cannot be distinguished. So, they simplified the problem for manifold-to-manifold transitions, which is valid for ions in glasses and, of course, crystals. Additional assumptions are needed to simplify the problem further, which are referred to as three and four to distinguish them from the first two assumptions made earlier.

3. All Stark levels within the ground manifold are equally populated.
4. The material is optically isotropic.

The third assumption is only reasonably met in most cases. There is actually a Boltzmann distribution of the population among the Stark levels. It becomes more valid the lower in energy the Stark splitting is. It also becomes more valid at higher temperatures. It is certainly a very bad assumption at low temperatures, and should not be applied to low temperature studies. The forth assumption is, of course, not valid for uniaxial or biaxial crystals. Nevertheless, polarization averaged studies can alleviate this restriction. These additional assumptions, while clear qualitatively, are often not made very clear in how they are carried out quantitatively, even in Judd's original article. To see how these assumptions are carried out in a quantitative way it is necessary to first define a quantity called the *oscillator strength*. The term oscillator strength is a historical term that has its origins relating to quantum mechanical resonance scattering in the Rutherford atomic model of a classically damped oscillator, and is directly related to a term called the *cross section*, for reasons originating in its introduction in atomic scattering theory. Nevertheless, these terms were historically adopted to describe transition intensities in the early days of studies of atomic transitions for their obvious connection to multipole transitions and their analogy to classical damped oscillators. The oscillator strength (f-number) for an electric dipole transition is defined as [3],

$$f = \frac{8\pi^2 mc}{h\bar{\lambda}e^2} n\left(\frac{n^2+2}{3n}\right)^2 \sum_{MM'} \left|\langle \alpha JM | \mathbf{P} | \alpha' J'M' \rangle\right|^2 \tag{22}$$

Squaring Eq. (16), assumption three allows the sum to be carried out a sum over M and M′, the Stark split levels. The orthogonality condition the for 3j symbols gives,

$$\sum_{MM'} \begin{pmatrix} J & \lambda & J' \\ -M & Q & M' \end{pmatrix} \begin{pmatrix} J & \lambda' & J' \\ -M & Q' & M' \end{pmatrix} = \frac{1}{2\lambda+1} \delta_{\lambda\lambda'} \delta_{QQ'} \tag{23}$$

and a factor 1/(2J+1) is introduced since M = -J, -(J-1), ..., 0, ..., (J-1), J. Assumption four allows the sum over q, the polarization. The orthogonality condition for the 3j symbols gives,

$$\sum_{q} \begin{pmatrix} 1 & t & \lambda \\ q & p & Q \end{pmatrix} \begin{pmatrix} 1 & t' & \lambda \\ q & p' & Q \end{pmatrix} = \frac{1}{2t+1} \delta_{tt'} \delta_{pp'} \tag{24}$$

and a factor of 1/3 is introduced since q = 0 for π polarization (E ⊥ c) and q = ±1 for σ polarization (E || c). In other words there are three values of q, one for π polarization and two for σ polarization. So, the summations over M, M′ and q are carried out, leaving only the summations over λ, p and t. The result for the oscillator strength is,

$$f = \frac{8\pi^2 mc}{3h\bar{\lambda}(2J+1)} n\left(\frac{n^2+2}{3n}\right)^2 \sum_{\lambda=2,4,6} \sum_{p} \sum_{t=1,3,5} (2\lambda+1) \frac{|A_{tp}|^2}{(2t+1)} Y^2(t,\lambda) \left|\left\langle \varphi_a \left\| \mathbf{U}^{(\lambda)} \right\| \varphi_b \right\rangle\right|^2 \qquad (25)$$

The sum is over λ = 2, 4, 6 and t = 1, 3, 5. This result can now be condensed into its final form. The Judd-Ofelt parameters can be defined as,

$$\Omega_\lambda = (2\lambda+1) \sum_{p} \sum_{t=1,3,5} \frac{|A_{tp}|^2}{(2t+1)} Y^2(t,\lambda) \qquad (26)$$

The Ω_λ, therefore, consist of odd-order parameters of the crystal field, radial integrals over wavefunctions of the $4f^n$ and perturbing, opposite parity wavefunctions of higher energy, and energies separating these states in terms of perturbation energy denominators. $Y(t,\lambda)$ was given previously in Eq. (17). With this substitution, the oscillator strength can be written as,

$$f = \frac{8\pi^2 mc}{3h\bar{\lambda}(2J+1)} n\left(\frac{n^2+2}{3n}\right)^2 \sum_{\lambda=2,4,6} \Omega_\lambda \left|\left\langle \varphi_a \left\| \mathbf{U}^{(\lambda)} \right\| \varphi_b \right\rangle\right|^2 \qquad (27)$$

The summation over λ is known as the *linestrength*. It is Eq. (6) given at the beginning of this section. This is the approximate solution of the Judd-Ofelt theory. It is often used to find ED matrix elements between mixed parity states for manifold-to-manifold transitions.

In principle it is possible to calculate the Judd-Ofelt parameters *ab-initio*, but this requires accurate values for the radial integrals and odd-order crystal field components, which are not known to a high enough degree of precision. What is usually done is to treat the Judd-Ofelt parameters as a set of phenomenological parameters to be determined from fitting experimental absorption measurements determined in Eq. (28) with the theoretical Judd-Ofelt expression in Eq. (6). This is the subject of the next section. The Judd-Ofelt theory in practice.

4. Judd-Ofelt Theory : Practices

The Judd-Ofelt theory [11,12] allows for the calculation of manifold to manifold transition probabilities, from which the radiative lifetimes and branching ratios of emission can be determined. A Judd-Ofelt analysis relies on accurate absorption measurements, specifically the integrated absorption cross section over the wavelength range of a number of manifolds. From the integrated absorption cross section, the so-called linestrength, S_m, can be found,

$$S_m = \frac{3ch(2J+1)}{8\pi^3 e^2 \bar{\lambda}} n\left(\frac{3}{n^2+2}\right)^2 \int_{manifold} \sigma(\lambda) d\lambda \tag{28}$$

where J is the total angular momentum of the initial ground manifold, found from the $^{2S+1}L_J$ designation. $\sigma(\lambda)$ is the absorption cross section as a function of wavelength. The mean wavelength, $\bar{\lambda}$, can be found from the first moment of the absorption cross section data,

$$\bar{\lambda} = \frac{\sum \sigma(\lambda)}{\sum \lambda \sigma(\lambda)} \tag{29}$$

In practice, the Judd-Ofelt theory is used to determine a set of phenomenological parameters, Ω_λ (λ = 2, 4, 6), by fitting the experimental absorption, Eq. (28), or emission measurements, in a least squares difference sum, with the Judd-Ofelt expression, Eq. (6). This is most efficiently done in the following way. First, the linestrength in Eq. (28) is written as a 1xN column matrix, S_j^m, and Eq. (6) is also written in matrix form as,

$$S_j' = \sum_{i=1}^{3} M_{ij} \Omega_i \tag{30}$$

where M_{ij} are components of a N x 3 matrix for the square matrix elements of $U^{(2)}$, $U^{(4)}$ and $U^{(6)}$. The Ω_κ are components of a 1 x 3 matrix for the Judd-Ofelt parameters Ω_2, Ω_4 and Ω_6. Note that N represents the number of transitions to fit, which depends on the number of absorption manifolds actually measured. Obviously, since there are only three Judd-Ofelt parameters, N > 3. For example, since Ytterbium (Yb) has only has one absorption manifold, the Judd-Ofelt theory cannot be applied to Yb. Next, the sum of the squared difference is formed,

$$\sigma^2 = \sum_{j=1}^{N} \left(S_j^m - \sum_{i=1}^{3} M_{ij} \Omega_i \right)^2 \tag{31}$$

and minimized by taking the derivative with respect to Ω and setting the result equal to zero,

$$\frac{\partial(\sigma^2)}{\partial \Omega_k} = -2 \sum_{j=1}^{N} M_{jk} \left(S_j^m - \sum_{i=1}^{3} M_{ij} \Omega_i \right) = 0 \tag{32}$$

The set of Judd-Ofelt parameters that minimizes the sum of the squared difference of measured and theoretical linestrength is written in matrix form, $\mathbf{\Omega}^{(0)} = (\mathbf{M}^\dagger \mathbf{M})^{-1} \mathbf{M}$, where $\mathbf{M}^\dagger$ is the adjoint of $\mathbf{M}$. Due to the large number of calculations to be made, matrices are suitable for

computer based calculations. Once the Judd-Ofelt parameters are determined, they can be used to calculate transition probabilities, A(J;J′), of all excited states from the equation,

$$A(J';J) = \frac{64\pi^4 e^2}{3h(2J'+1)\bar{\lambda}^3}\left[n\left(\frac{n^2+2}{3}\right)^2 S_{ED} + n^2 S_{MD} \right] \tag{33}$$

where n is the refractive index of the solid, S_{ED} and S_{MD} are the electric and magnetic dipole line strengths, respectively. In this equation J′ is the total angular momentum of the upper excited state. Electric dipole linestrengths, S_{ED}, are calculated from each excited manifold to all lower lying manifolds from Eq. (6) using the matrix elements, $U^{(\lambda)}$, and Judd-Ofelt parameters.

Magnetic dipole linestrengths are calculated in a straightforward way from angular momentum considerations [15]. These values are then converted to intermediate coupling using free ion wavefunctions. The calculation of magnetic dipole linestrengths, S_{MD}, in intermediate coupling has been discussed in a previous article by the author [16]. The matrix elements for MD transitions are nonzero only if S = S′, and L = L′. Additional selection rules exist for the total angular momentum J. They are J = J′, J = J′ + 1, and J = J′ – 1. These selection rules were shown in figure 6. Calculation of magnetic dipole matrix elements is fairly straightforward. For a given S, L and J of the initial state, the matrix elements in LS-coupling are calculated from relations derived from angular momentum considerations. In the LS-coupling scheme, the matrix elements for the angular momentum operator **L** and the spin operator **S** are:

$$\left\langle f^n SLJ \left\| \mathbf{L} \right\| f^n S'L'J' \right\rangle = (-1)^{S+L+J+1} \begin{Bmatrix} S & L & J \\ 1 & J' & L \end{Bmatrix} \sqrt{L(L+1)(2L+1)(2J+1)(2J'+1)} \tag{34}$$

$$\left\langle f^n SLJ \left\| \mathbf{S} \right\| f^n S'L'J' \right\rangle = (-1)^{S+L+J+1} \begin{Bmatrix} S & L & J \\ J' & 1 & S \end{Bmatrix} \sqrt{S(S+1)(2S+1)(2J+1)(2J'+1)} \tag{35}$$

Expansion of the 6j symbols and combining Eq. (34) and Eq. (35) leads to the following equations for the MD matrix elements between LS-coupled states states:

$$\left\langle f^n SLJ \left\| \mathbf{L} + 2\mathbf{S} \right\| f^n S'L'J \right\rangle = \left[S(S+1) - L(L+1) + 3J(J+1) \right] \left[\frac{2J+1}{4J(J+1)} \right]^{1/2} \tag{36}$$

$$\left\langle f^n SLJ \left\| \mathbf{L} + 2\mathbf{S} \right\| f^n S'L'J-1 \right\rangle = \left\{ \left[(S+L+1)^2 - J^2 \right] \left[\frac{J^2 - (L-S)^2}{4J} \right] \right\}^{1/2} \tag{37}$$

$$\left\langle f^n SLJ \left\| \mathbf{L} + 2\mathbf{S} \right\| f^n S'L'J+1 \right\rangle = \left\{ \left[(S+L+1)^2 - (J+1)^2 \right] \left[\frac{(J+1)^2 - (L-S)^2}{4(J+1)} \right] \right\}^{1/2} \tag{38}$$

These matrix elements cannot be used directly for rare earth ions. The reason is that the LS-coupling scheme is inapplicable to rare earth ions because the interaction between electrons in the $4f$ shell and the spin orbit interaction are of the same order of magnitude. It is necessary, therefore, to find the matrix elements in another coupling scheme. Fortunately, this is easily achieved by choosing the basis states as a linear combination of LS coupling states. In this intermediate coupling scheme, which treats the electron interactions and spin-orbit interactions as being approximately the same order of magnitude, the new wavefunctions are,

$$\left| f^n [SL] J \right\rangle = \sum_{SL} C(S,L) \left| f^n SLJ \right\rangle \tag{39}$$

The coefficients C(S,L) are found by diagonalizing the combined electrostatic, spin-orbit and configuration-interaction matrices to obtain intermediate-coupled wavefunctions. MD transitions in intermediate coupling are possible if pairs of LS-coupled states are formed that satisfy MD selection rules. The MD matrix elements in intermediate coupling now follow from,

$$\left\langle f^n [SL] J \| \mathbf{L} + 2\mathbf{S} \| f^n [S'L'] J' \right\rangle = \sum_{SL,S'L'} C(S,L) C(S',L') \left\langle f^n SLJ \| \mathbf{L} + 2\mathbf{S} \| f^n S'L'J' \right\rangle \tag{40}$$

If the interest is only in manifold-to-manifold MD transition probabilities, then it is sufficient to use free ion intermediate-coupled wavefunctions to find coupling coefficients. The manifold-to-manifold wavefunctions of ions in crystals generally show only small departures from the free ion values since the crystal field is only a small perturbation. It is known that MD transitions are allowed between states of the same parity. They are generally orders of magnitude smaller than ED transitions in free ions, but since the ED radiation for ions in solids occurs as a result of a perturbation, the ED intensities are much smaller than in free ions. As a result, some magnetic dipole transitions will make significant contributions to the observed intensities. The strongest MD transitions will usually be in the infrared, but exceptions can be expected. All the tools have been developed up to this point, and it is now a simple matter to find the radiative lifetimes, τ_r, and the branching ratio, β,

$$\frac{1}{\tau_r} = \sum_J A(J';J) \tag{41}$$

$$\beta_{J'J} = \frac{A(J';J)}{\sum_J A(J';J)} \tag{42}$$

The procedure of a Judd-Ofelt analysis is represented in a simple flow chart shown in figure 7 below. This figure shows the major steps in the process, culminating in calculation of the transition probabilities and branching ratios. The details of all these steps have been covered and form, a hopefully clear and coherent, recipe for what is called a Judd-Ofelt analysis.

It is useful at this point to show an example illustrating a real Judd-Ofelt analysis and a test of its validity. Ho^{3+} ions in $LiYF_4$ (YLF) is chosen as an example as it represents a case in

extremes. YLF is a uniaxial host material exhibiting absorption that depends on polarization. Holmium also possesses many manifolds in its absorption spectra, some of which overlap with each other. This is a particularly good example because it illustrates that, despite these challenges, the Judd-Ofelt theory is remarkably accurate in most cases.

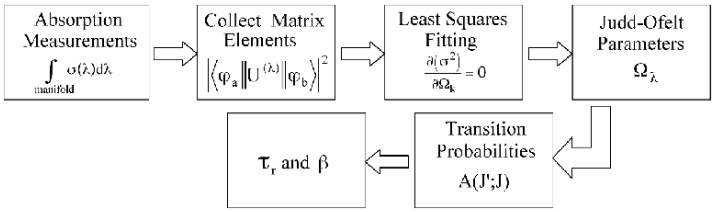

Figure 7. Procedure of Judd-Ofelt analysis.

The visible absorption spectrum of Ho:YLF is shown in figure 8. The π and σ polarized absorption cross sections of the manifolds shown in this figure were summed over wavelength and polarization averaged to obtain the integral in Eq. (28). The linestrengths were then calculated and these values were used in the Judd-Ofelt fitting. The results of the Judd-Ofelt fit are shown in table II. The measured and calculated linestrength values are shown in the right column of the table. The matrix elements and mean wavelength are also shown for convenience. The Judd-Ofelt parameters were found to be $\Omega_2 = 1.03 \times 10^{-20}$ cm^2, $\Omega_4 = 2.32 \times 10^{-20}$ cm^2, $\Omega_4 = 1.93 \times 10^{-20}$ cm^2. The root mean square (RMS) deviation, which is a measure of the overall quality of the fit, was found to be $\delta = 0.13 \times 10^{-20}$ cm^2.

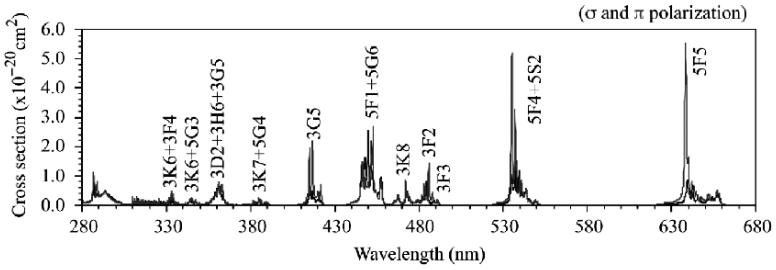

Figure 8. Visible absorption spectrum of Ho:YLF.

The Judd-Ofelt parameters can now be used to calculate the electric dipole transition probabilities between any excited manifold and any lower lying manifold. The magnetic dipole transition probabilities are calculated separately as discussed previously. The transition probabilities, ED and MD, then allow for calculation of branching ratios, β, and radiative lifetimes, τ_r. Table III collects the results for the Ho:YLF case being examined here.

Table II. Judd-Ofelt fitting in Ho^{3+} YLF.

Transition (from $^5I_8$)	$\|U^{(2)}\|^2$	$\|U^{(4)}\|^2$	$\|U^{(6)}\|^2$	$\bar{\lambda}$(nm)	Linestrength(10^{-20} cm^2)	
					measured	calculated
$^3K_6 + {}^3F_4$	0.0026	0.1263	0.0073	334	0.2639	0.3097
$^3L_9 + {}^5G_3$	0.0185	0.0052	0.1169	345	0.2920	0.3533
$^3D_2 + {}^3H_6 + {}^5G_5$	0.2155	0.1969	0.1679	360	1.2803	1.0023
$^3K_7 + {}^5G_4$	0.0058	0.0361	0.0697	385	0.2819	0.2243
$^5G_5$	0.0000	0.5338	0.0002	418	1.1086	1.2396
$^5F_1 + {}^5G_6$	1.5201	0.8410	0.1411	448	3.7492	3.7839
$^3K_8$	0.0208	0.0334	0.1535	467	0.2282	0.3952
$^3F_2$	0.0000	0.0000	0.2041	473	0.3488	0.3941
$^3F_3$	0.0000	0.0000	0.3464	486	0.7587	0.6689
$^5F_4 + {}^5S_2$	0.0000	0.2392	0.9339	540	2.5359	2.3587
$^5F_5$	0.0000	0.4250	0.5687	645	2.1426	2.0848
$^5I_5$	0.0000	0.0100	0.0936	886	0.1741	0.2039
$^5I_6$	0.0084	0.0386	0.6921	1175	1.1067	1.4347

Table III. Judd-Ofelt transition probabilities in Ho^{3+} YLF.

Transition	$\|U^{(2)}\|^2$	$\|U^{(4)}\|^2$	$\|U^{(6)}\|^2$	$\bar{\lambda}$ (nm)	S_{ED}[1]	A_{MD} (s^{-1})	A_{ED} (s^{-1})	β	τ_r (μs)
$^5F_4 \rightarrow {}^5S_2$	0.0000	0.0159	0.0033	67656	0.043		0.00	0.000	
$^5F_4 \rightarrow {}^5F_5$	0.1944	0.0923	0.0080	3173	0.429	2.83	2.82	0.002	
$^5F_4 \rightarrow {}^5I_4$	0.0001	0.0234	0.2587	1887	0.554		17.67	0.005	
$^5F_4 \rightarrow {}^5I_5$	0.0018	0.1314	0.4655	1327	1.206		111.33	0.033	
$^5F_4 \rightarrow {}^5I_6$	0.0012	0.2586	0.1697	986	0.930		207.79	0.062	
$^5F_4 \rightarrow {}^5I_7$	0.0000	0.1988	0.0324	738	0.524		284.43	0.084	
$^5F_4 \rightarrow {}^5I_8$	0.0000	0.2402	0.7079	536	1.925		2748.90	0.814	295
$^5S_2 \rightarrow {}^5F_5$	0.0000	0.0110	0.0036	3330	0.033		0.33	0.000	
$^5S_2 \rightarrow {}^5I_4$	0.0013	0.0279	0.2795	1942	0.606		31.92	0.016	
$^5S_2 \rightarrow {}^5I_5$	0.0000	0.0043	0.1062	1354	0.215		33.67	0.016	
$^5S_2 \rightarrow {}^5I_6$	0.0000	0.0206	0.1541	1000	0.345		133.16	0.065	
$^5S_2 \rightarrow {}^5I_7$	0.0000	0.0000	0.4096	746	0.791		747.45	0.366	
$^5S_2 \rightarrow {}^5I_8$	0.0000	0.0000	0.2270	540	0.438		1100.01	0.538	489
$^5F_5 \rightarrow {}^5I_4$	0.0001	0.0059	0.0040	4658	0.015		0.03	0.000	
$^5F_5 \rightarrow {}^5I_5$	0.0068	0.0271	0.1649	2282	0.252		5.70	0.003	
$^5F_5 \rightarrow {}^5I_6$	0.0102	0.1213	0.4995	1430	0.818		74.62	0.041	
$^5F_5 \rightarrow {}^5I_7$	0.0177	0.3298	0.4340	961	1.080		324.00	0.180	
$^5F_5 \rightarrow {}^5I_8$	0.0000	0.4277	0.5686	645	1.390		1394.42	0.776	556
$^5I_4 \rightarrow {}^5I_5$	0.0312	0.1237	0.9099	4472	2.076	1.94	4.69	0.079	
$^5I_4 \rightarrow {}^5I_6$	0.0022	0.0281	0.6640	2064	1.350		32.11	0.381	
$^5I_4 \rightarrow {}^5I_7$	0.0000	0.0033	0.1568	1211	0.310		37.75	0.448	
$^5I_4 \rightarrow {}^5I_8$	0.0000	0.0000	0.0077	749	0.015		7.72	0.092	11875
$^5I_5 \rightarrow {}^5I_6$	0.0438	0.1705	0.5729	3831	1.547	4.07	4.44	0.067	
$^5I_5 \rightarrow {}^5I_7$	0.0027	0.0226	0.8887	1662	1.771		67.93	0.538	
$^5I_5 \rightarrow {}^5I_8$	0.0000	0.0099	0.0936	899	0.204		49.79	0.394	7922
$^5I_6 \rightarrow {}^5I_7$	0.0319	0.1336	0.9308	2934	2.140	8.11	12.78	0.135	
$^5I_6 \rightarrow {}^5I_8$	0.0083	0.0383	0.6918	1175	1.433		134.03	0.865	6455
$^5I_7 \rightarrow {}^5I_8$	0.0249	0.1344	1.5217	1960	3.276	15.91	55.92	1.000	13921

[1]Line strength values are in units $10^{-20} cm^2$.

It is now prudent to ask how good the results are, that is, does the Judd-Ofelt theory accurately predict the branching ratios and radiative lifetimes? A method for testing the Judd-Ofelt theory is therefore needed. The simplest way is to just measure the branching ratios and radiative lifetimes. Branching ratios can be directly measured from emission spectra, as they are just the fraction of the total photon flux from an upper to lower manifold. Selected manifold to manifold branching ratios in Ho:YLF are shown in table IV. The agreement between measurement and the Judd-Ofelt theory is quite good, the error being less than 15%.

Table IV. Measured and calculated branching ratios in Ho^{3+} YLF.

Ion	Transition	Wavelength range (nm)	$\beta_{measured}$	$\beta_{Judd-Ofelt}$	Percent difference
Ho	$^5S_2 \rightarrow {}^5I_6$	1014 – 1032	0.0543	0.0633	14.2
Ho	$^5S_2 \rightarrow {}^5I_7$	747 – 758	0.2540	0.2247	11.5
Ho	$^5S_2 \rightarrow {}^5I_8$	539 – 559	0.6916	0.6759	2.3
Ho	$^5F_5 \rightarrow {}^5I_7$	952 – 981	0.1541	0.1801	14.4
Ho	$^5F_5 \rightarrow {}^5I_8$	638 – 659	0.8458	0.7752	8.3
Ho	$^5I_8 \rightarrow {}^5I_7$	1618 – 1681	0.6174	0.5381	12.8
Ho	$^5I_5 \rightarrow {}^5I_8$	882 – 915	0.3822	0.3944	3.1

The radiative lifetimes are a bit more problematic because they are not directly measurable in most cases. The reason for this is that other processes besides spontaneous emission are usually present. These processes include energy transfer, nonradiative relaxation and radiative trapping, for example. So, directly measuring the lifetime will not always yield the radiative lifetime, even at low temperature. An alternate method is needed. Utilizing the reciprocity of absorption and emission, however, the radiative lifetimes can be indirectly derived. The emission cross section is related to the absorption cross section by the following equation originally derived by McCumber [17] and reformulated by Payne et al. [18],

$$\sigma_{em}(\lambda) = \sigma_{ab}(\lambda)\frac{Z_l}{Z_u}\exp\left[\left(E_{ZL} - \frac{hc}{\lambda}\right)\Big/ kT\right] \tag{43}$$

where Z_l and Z_u are the partition functions of the lower and upper manifolds, respectively. E_{ZL} is the zero-line energy, and is defined as the energy difference between the lowest Stark level of the upper manifold and the lowest Stark level of the lower manifold. An emission cross section derived from the absorption cross section in this way can be compared to an actual measured emission cross section. The measured emission cross section is given by the equation [19],

$$\sigma(\lambda) = \frac{\lambda^5}{8\pi c n^2 (\tau_r / \beta)} \frac{3I_\alpha(\lambda)}{\int [2I_\sigma(\lambda) + I_\pi(\lambda)]\lambda d\lambda} \tag{44}$$

where $I_\alpha(\lambda)$ is the emission intensity for α (π or σ) polarization, τ_r is the radiative lifetime, β is the branching ratio, and n is the index of refraction. Note that $I_\sigma(\lambda) = I_\pi(\lambda)$ for isotropic crystals.

By scaling the factor τ_r/β such that equations (43) and (44) agree, the radiative lifetime can be extracted and then compared to the values calculated in the Judd-Ofelt theory. A pictorial representation of this process is shown in figure 9 for the lowest excited state in Ho, the $^5I_7$ manifold. The top set of spectra, a and b, show the measured π and σ absorption spectra. The middle set, c and d, show the π and σ emission derived from absorption using Eq. (43). The bottom set, e and f, show the measured π and σ emission from Eq. (44) scaled to match the derived emission with a value of τ_r/β = 14000 μs. The branching ratio in this case is one, so the radiative lifetime is 14 ms. For other manifolds, a measurement of the branching ratio must be made. Alternatively, a Judd-Ofelt branching ratio can also be used if the measurement cannot be done, but since this is a test of the Judd-Ofelt theory, this defeats the purpose of the test somewhat. However, if there is good agreement between the β's that can be measured and those determined in the Judd-Ofelt theory, then this improves confidence in using Judd-Ofelt β's for those that cannot be measured. The radiative lifetimes derived from reciprocity and those calculated from the Judd-Ofelt theory are shown in table V. The result is that the error is less than 30% for the radiative lifetimes. So, the Judd-Ofelt theory is valid within 15 to 30% as a liberal estimate. A more conservative estimate puts the error in the range of 10 to 20%.

Table V. Measured and calculated radiative lifetimes in Ho^{3+} YLF.

Ion	Transition	β	$\tau_{measured}$ (μs)	$\tau_{Judd-Ofelt}$ (μs)	percent difference
Ho	$^5F_4+^5S_2 \rightarrow {}^5I_8$	0.6916	258 – 530	295 – 542	2.2 – 12.5
Ho	$^5F_5 \rightarrow {}^5I_8$	0.8458	677	556	17.8
Ho	$^5I_5 \rightarrow {}^5I_8$	0.3822	5790	7922	26.9
Ho	$^5I_6 \rightarrow {}^5I_8$	0.8651	6592	6455	2.0
Ho	$^5I_7 \rightarrow {}^5I_8$	1.0000	14000	13921	0.5

The results that have been shown here are consistent with the general consensus of the accuracy of the Judd-Ofelt theory. Usually such errors have been only approximations in the past. This analysis here shows a concrete example with definative numbers to assess the accuracy. In considering the starting point of the theory, the approximations made and the simplifications used to reduce the problem to something that can be straightforwardly calculated, this is really quite remarkable. In a sense it is a testament to simple and reasonable assumptions and approximations made with a physical basis for their implementation.

In the remaining section, some special cases where the Judd-Ofelt theory encounters problems are discussed. The lanthanide ions praseodymium and europium are discussed. These problems with the standard Judd-Ofelt theory, as discussed in the next section, lead to extensions of the Judd-Ofelt theory. These extensions are briefly outlined and indications are made, where appropriate, how these extensions may explain some problems with the standard theory, especially in the case of some europium transitions. Finally, some remaining problems towards future direction are also outlined. These are problems not yet resolved and indicate a further need for future work on this very fascinating topic.

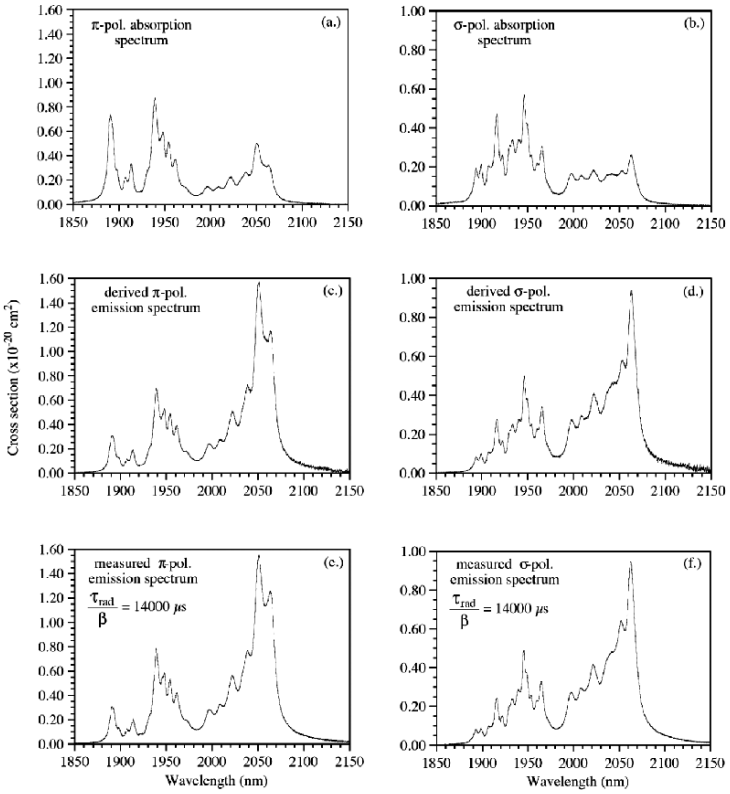

Figure 9. Cross sections of the $^5I_7$ manifold in Ho:YLF.

5. Beyond the Standard Judd-Ofelt Theory

5.1. THE CASE OF PRASEODYMIUM

Praseodymium ions suffer from several problems in applying the Judd-Ofelt theory. There are often large deviations between calculations and experimental observations, exhibited by the large RMS values obtain in Judd-Ofelt fitting. In addition, the Judd-Ofelt parameters obtained for Pr doped materials tend to be very dependent on the transitions used in the fit. Sometimes negative values are obtained for Ω_2, in opposition to its definition as given in Eq. (26). These inconsistencies are usually explained by the small difference in the average energies, $\approx$ 50,000 cm^{-1},

between the $4f^n$ and $4f^{(n-1)}5d$ configurations in Pr^{3+} ions. Remember that the first two assumptions of the Judd-Ofelt theory took the perturbing configurations to be degenerate and well separated from the f-f transitions of the $4f^n$ configuration. There have been several approaches to these problems. Dunnina, *et al*. [20] modified the standard Judd-Ofelt theory to take into account the finite 4f5d energy,

$$\Omega'_\lambda = \Omega_\lambda \left[1 + \left(\Delta E_{ij} - 2\bar{E}_{4f} \right) \Big/ \left(E^0_{5d} - \bar{E}_{4f} \right) \right] \tag{45}$$

where E_i and E_j are the initial and final states of the $4f$ transition, $\bar{E}_{4f}$ is the average energy of the $4f$ states, and E^0_{5d} is the lowest energy of the $4f5d$ state. This modified theory has been used with some success to eliminate the problem of negative Ω_2. Quimby *et al*. [21] has applied a modified Judd-Ofelt theory by introducing fluorescence branching ratios. This allows the Judd-Ofelt parameters to be reliably calculated with fewer ground state absorption measurements than would otherwise be necessary, but requires additional fluorescence measurements. These methods were applied to Pr:ZBLAN glass and produced fairly good agreement between the calculated and measured oscillator strengths. However, Goldner *et al*. [22] has argued that such modified theories are not really necessary and, in fact, do not improve the fit substantially if reasonable values for the $4f5d$ energies are used. Goldner *et al*. showed that by using a normalized least squares fitting, the measurements are properly scaled according to the error associated with each one, and positive, stable parameters are obtained with improved RMS deviations. In this new fitting procedure, Eq. (31) is replaced with,

$$\sigma^2 = \sum_{j=1}^{N} \left[\left(S_j^m - \sum_i M_{ij} \Omega_i \right) \Big/ \sigma_i \right]^2 \tag{46}$$

where σ_i are the standard deviations on the absorption measurements. This modified fitting procedure has the advantage that transitions measured with the same accuracy have the same weight in the fit. This prohibits stronger transitions from dominating the fit. In addition, there is no need to modify the Judd-Ofelt theory itself to obtain better fits with stable, positive parameters in Pr^{3+} doped materials.

5.2. THE CASE OF EUROPIUM

Europium ions provide another challenge to the standard Judd-Ofelt theory. In particular, the transitions $^7F_0 \leftrightarrow {}^5D_{Jodd}$, $^7F_{Jodd} \leftrightarrow {}^5D_0$ and $^7F_0 \leftrightarrow {}^5D_0$ are forbidden transitions in the Judd-Ofelt theory. They violate the selection rules derived earlier and illustrated in figure 6. Some of these transitions are primarily magnetic dipole in nature, but do occur as electric dipole transitions with low intensity in some materials. In general, for the other lanthanide ions as well, all $J = 0$ to $J' = 0$ transitions are forbidden, as well as transitions with $\Delta S = 1$. Although the later are spin-forbidden in the Judd-Ofelt theory, they account for a substantial number of observed

transitions of lanthanide ions in solids. Clearly, this implies that the Judd-Ofelt theory is incomplete in its standard form. The transitions in the Eu^{3+} ion, therefore, provide an ideal testing ground for possible extensions to the standard theory. Spin-forbidden transition intensities have been treated by Burdick and Downer [23,24], where they show that spin forbidden transitions acquire a major fraction of their intensities from previously neglected spin-orbit linkages with excited configurations. In the intermediate coupling approximation, these linkages can contribute significantly when the spin-orbit interaction is comparable to the electrostatic interaction. This excited state spin-orbit interaction is known as the Wybourne-Downer mechanism. Tanaka and Kushida have covered the 0-0, 0-even, and 0-odd transitions for Eu^{3+} ions in a number of papers [25,26,27,28]. Some of these discuss the interference of J-mixing and spin-orbit effects. The europium ion continues to lend itself to testing new assumptions regarding the prevalent interactions of ions in solids and how they affect the intensities in the context of modifying the Judd-Ofelt theory towards a more complete theoretical description.

5.3. EXTENSIONS TO THE JUDD-OFELT THEORY

Since the original formulation of the Judd-Ofelt theory in 1962, there have been many investigations into extending the theory to explain its shortcomings. Some of these shortcomings have been discussed in the last two subsections. These shortcomings extend to other lanthanides besides the ones discussed here. The shortcomings have more to do with the peculiar nature of certain transitions. This topic cannot be discussed in all its details and subtleties here, as it is quite extensive. What follows is an outline of the basic mechanisms that have been considered to explain the shortcomings of the standard Judd-Ofelt theory.

1. *J-Mixing*: The wavefunctions of the $J \neq 0$ state are mixed into the $J = 0$ state by the crystal field potential. This mechanism goes beyond the free-ion model and has been used, for example, to explain the $^5D_0 \rightarrow {}^7F_0$ and $^7F_{Jodd}$ transitions in Eu^{3+} [25,29,30].

2. *Electron Correlation*: The electrostatic interaction between electrons is taken into account. This goes beyond the single configuration approximation in the standard Judd-Ofelt theory. Electron correlation within the 4f shell is used to set a theoretical description of 0-0 and 0-1 transitions in Eu^{3+} ions in hosts with C_{2v} symmetry [31].

3. *Dynamic Coupling*: The mutual interaction of the lanthanide ion and the crystal environment is taken into account. This mechanism goes beyond the static coupling model in the standard Judd-Ofelt theory and is explains hypersensitive transitions, that is, transitions which are highly dependent on changes in host environment [32,33,34].

4. *Wybourne-Downer Mechanism*: This mechanism involves spin-orbit interaction among states of the excited configurations, leading to an admixing of spin states into the $4f^n$ configuration. Originally proposed by Wybourne [35], it has been used to explain $\Delta S = 1$ spin forbidden transitions [23,24].

5. *Relativistic Contributions*: Involves a relativistic treatment of f-f transitions in crystal fields. This reformulation of the crystal field and operators in relativistic terms is a recent advancement and future calculations will indicate their significance, especially for the heavier actinides [36,37,38].

Two extensive review articles covering the intensities of f-f transitions are available in the literature. The early development of the Judd-Ofelt theory can be found in an article by Peacock [39]. More recent developments can be found in a review article by Smentek [40]. In addition, the reader is encouraged to look at the 2003 special issue of *Molecular Physics* [41] commemorating the 40th anniversary of the Judd-Ofelt theory. This volume contains many interesting articles on the state of knowledge of Judd-Ofelt theories and their applications.

5.4. FUTURE DIRECTIONS

The Judd-Ofelt theory as originally formulated is a second-order approach that treats the odd-order terms of the crystal field as a perturbation. This perturbing influence allows mixing of opposite parity states from higher lying configurations to be mixed into $4f$ states, producing mixed parity states between which electric dipole transitions become allowed. This formulation is based on the static, free-ion and single configuration approximations as discussed in section 3. In the last few subsections, it was seen that there is a need to extend the Judd-Ofelt theory to account for anomalous transitions. The various operators used to represent any additional physical mechanisms are considered in the perturbation expansion not just to second-order, but in third-order as well. It is difficult, if not impossible, to say what the relative importance of each mechanism is. In fact, the appearance of a term in third-order may have more impact than a term occurring in second-order. This remains an outstanding problem for future development. It results in a very complicated situation to disentangle which mechanisms are relevant and physically significant. The multitude of mechanisms that can be realized produces a situation that departs markedly from the simple approximations and assumptions of the standard Judd-Ofelt theory and will continue to be a challenge in the future. In fact, by extending the Judd-Ofelt theory, the simple linear parametric fitting is lost and physically meaningful descriptions can easily be obscured.

Another area of future direction is in the area of *ab-initio* calculations. Such calculations are still not entirely successful in explaining all aspects of the intensities of f-f transitions. The availability of accurate Hartree-Fock relativistic radial integrals has helped the situation, but there remains a lack of accurate knowledge of the odd-order crystal field parameters. This has hampered the development of *ab-initio* theories to some extent. Further, there is the issue of the vibrational-electronic coupling which complicates the spectral dynamics. It is clear that the theory of f-f transitions is not yet complete. As Professor Brian G. Wybourne has said, *"The Judd-Ofelt theory marked a turning point in our understanding of the fascinating spectroscopic properties of the rare earths. It has been in a very real sense the first step in the journey to an understanding of the rare-earths and their heavier cousins, the actinides, but like many journeys into the unknown, the end is not in sight"* [1].

6. Appendix

There are many interesting sidelines, or further journeys, that could be taken in learning this very fascinating subject. It is not possible to cover everything here in this article, but it is worthwhile to point out a few extra sidelines that might be of interest to the reader here in the appendix. The articles of Kushida [42,43,44] provide an interesting perspective on energy transfer theory in the context of Judd-Ofelt theory. The articles of Peacock [45,46,47,48] cover a variety of topics including vibronic transitions, Judd-Ofelt parameter variation over isostructural series and sensitivity of Judd-Ofelt parameters to transitions used. Peacock's review article [39] discusses a wide variety of topics on the Judd-Ofelt theory. Jorgensen and Reisfeld [49,50] have discussed the Judd-Ofelt parameters and chemical bonding of lanthanide ions to the solid host material. The Judd Ofelt parameter, Ω_2, is affected by covalent bonding, while Ω_6 is related to the rigidity of the solid host in which the lanthanide ions are situated. The work of Edvardsson and co-worker's [51,52,53,54,55] should not escape attention here. There are some very interesting results discussed in the context of their Molecular Dynamics Simulations. Finally, there are many articles by L. Smentek, too numerous to mention here. She has written extensively on the Judd-Ofelt theory. Her review article [40] is especially thorough. Many references to earlier works can be found in this review article. See also the 2003 special issue of *Molecular Physics* [41], celebrating the 40th anniversary of the Judd-Ofelt theory.

In the remainder of this appendix, a computer program is given. This program, written in BASIC, provides the core routines for creating a Judd-Ofelt analysis program. A full version of the program with input files can be provided on request (Brian.M.Walsh@nasa.gov).

```
REM: BEGIN JUDD-OFELT FITTING ROUTINE
REM: WRITTEN BY BRIAN M. WALSH
REM: GET INITIAL INPUT
FOR I=0 TO NI: REM NI=NUMBER OF TRANSITIONS MEASURED -1
      INPUT TAGS :  REM (2J+1) OF TERMINAL LEVEL (GROUND STATE)
      INPUT IA(I) : REM INTEGRATED ABSORPTION IN UNITS 10^-20 CM^2-NM
      INPUT W(I) :  REM AVERAGE WAVELENGTH OF TRANSITION IN NM
      INPUT NS(I) : REM INDEX OF REFRACTION AT WAVELENGTH W(I)
      FOR COL= 0 TO 2 : REM ONLY 3 COLUMNS FOR U(2), U(4), U(6)
            INPUT M(NI , COL) : REM REDUCED MATRIX ELEMENTS
      NEXT COL
      REM: FIND THE LINESTRENGTH SE(I)
      SE(I) = IA(I) * 10.41 * NS(I) * (3 / (NS(I)^2 + 2))^2 * TAGS / W(I)
      REM NOTE THAT 3hc/8π^3e^2 = 10.41
NEXT I
"100" REM JUDD-OFELT LEAST SQUARES FIT FOR ABSORPTION LINE STRENGTHS
"200" REM GET TRANSPOSE OF MATRIX COMPOSED OF REDUCED MATRIX ELEMENT'S [ME]
FOR I = 0 TO NJ: REM NJ = 2, ONLY 3 ARRAY ELEMENTS FOR U(2), U(4), U(6)
      FOR J = 0 TO NI
            A(I , J) = ME(J , I)
      NEXT J
NEXT I
"300" REM MULTIPLY TRANSPOSE [A] BY ORIGINAL MATRIX [ME]
FOR I = 0 TO NJ
      FOR J = 0 TO NJ
            FOR K = 0 TO NI
                  AN(I , J) = AN(I , J) + A(I , K) * ME(K , J)
            NEXT K
      NEXT J
NEXT I
"400" REM INVERT MATRIX [AN]
N=NJ + 1
FOR K = 0 TO N - 1
      FOR I = 0 TO N - 1
            AN(I , N) = ABS(I = K)
```

```
        NEXT I
        FOR J = 1 TO N
                AN(K , J) = AN(K , J) / AN(K , 0)
                FOR I = 0 TO N-1
                        IF I = K THEN GOTO "410"
                        AN(I , J) = AN(I , J) - AN(K , J) * AN(I , 0)
"410"           NEXT I
        NEXT J
        FOR I = 0 TO N - 1
                FOR J = 0 TO N - 1
                        AN(I , J) = AN(I , J+1)
                NEXT J
        NEXT I
NEXT K
"500" REM MULTIPLY INVERSE [AN] BY TRANSPOSE [A]
FOR I = 0 TO NJ
        FOR J = 0 TO NI
                FOR K = 0 TO NJ
                        AF(I , J) = AF(I , J) + AN(I , K) * A(K , J)
                NEXT K
        NEXT J
NEXT I
"600" REM FIND JUDD-OFELT PARAMETERS [JO]
FOR I = 0 TO NJ
        FOR J = 0 TO NI
                JO(I) = JO(I) + AF(I , J) * SE(J)
        NEXT J
NEXT I
"700" REM FIND THEORETICAL LINE STRENGTHS [ST]
FOR I = 0 TO NI
        FOR J = 0 TO NJ
                ST(I) = ST(I) + ME(I , J) * JO(J)
        NEXT J
NEXT I
"800" REM FIND RMS DEVIATION
FOR I = 0 TO NI
        SSUM = SSUM + (SE(I) - ST(I))^2
NEXT I
SSUM = SSUM / (NI - 2) : REM NUMBER OF TRANSITIONS (NI + 1) > 3
RMS = SQR(SSUM) : ROOT MEAN SQUARE ERROR
"900" CALCULATE EXCITED STATE TRANSITION PROBABILITIES
FOR I = 0 TO NI - 1
        FOR K = I + 1 TO NI
                WT(K) = ABS(WL(I) - WL(K)) : REM TRANSITION WAVELENGTH IN NM
                INPUT U(0 , I),U(1 , I),U(2 , I) : REM  GET MATRIX ELEMENTS FOR EACH TRANSITION
                INPUT TAES(I) : REM (2J + 1) OF EXCITED LEVEL
                FOR J = 0 TO NJ
                        TS(K) = TS(K) + U(J , I) * JO(J) : TRANSITION STRENGTH
                NEXT J
                AED(K)=7.23E10 * NS(K) * ((NS(K)^2 +2 )/3)^2 * (TS(K) * 1E-20)/(TAES(I) * (WT(K)*1E-7)^3)
                REM NOTE THAT 64π^4e^2/3hc = 7.23E10 CM/SEC.
                REM NOTE ALSO THAT LINESTRENGTHS HAVE UNITS OF 10^-20 CM^2
                REM HENCE THE 1E-20 FACTOR MULTIPLYING TS(K).
                RS = RS + AED(K) : REM RUNNING SUM OF TRANSITION PROBABILITIES
        NEXT K
        REM CALCULATE BRANCHING RATIOS
        FOR J = I + 1 TO K - 1
                BRATIO = AED(J)/RS: REM BRANCHING RATIO
        NEXT J
        REM CALCULATE LIFETIMES (INVERSE OF SUM OVER AED FOR ALL LOWER MANIFOLDS)
        FOR KK = 1 TO NI
                AEDSUM = 0
                FOR JJ = 1 TO KK
                        AEDSUM=AED(JJ)+AEDSUM: REM SUM  TRANSITION PROBABILITIES
                NEXT JJ
               AEDSUM(KK) = AEDSUM
                IF AEDSUM = 0 THEN GOTO "910"
                LIF(KK) = (1/AEDSUM(KK)) * 1000: REM RADIATIVE LIFETIME IN MILLISECONDS
"910" NEXT KK
REM ALL LINESTRENGTHS AND JUDD-OFELT PARAMETERS ARE IN UNITS OF 10^-20 CM^2
NEXT I
```

Acknowledgements

I wish to extend my thanks to Prof. Baldassare Di Bartolo, his staff, Prof. John Collins and Mr. Ottavio Forte, as well as the Majorana Center, for my participation in this year's course. I also wish to extend my sincere thanks to Ms. Regine DeWees for many thoughtful discussions and for her support during the preparation of my lectures.

References

1. Wybourne, B.G. (2004) The fascination of Rare earths-then, now and in the future, *J. Alloys and Compounds* **380**, 96-100.
2. Van Vleck, J. H. (1937) The puzzle of rare earth spectra in solids, *J. Phys. Chem.* **41**, 67-80.
3. Broer, L.F.J., Gorter, C.J, and Hoogschagen, J. (1945) On the intensities and the multipole character in the spectra of rare earth ions, *Physica* **XI**, 231-249.
4. Racah, G. (1941) Theory of complex spectra. I., *Phys. Rev.* **61**, 186-197.
5. Racah, G. (1942) Theory of complex spectra. II., *Phys. Rev.* **62**, 438-462.
6. Racah, G. (1943) Theory of complex spectra. III., *Phys. Rev.* **63**, 367-382.
7. Racah, G. (1949) Theory of complex spectra. IV., *Phys. Rev.* **76**, 1352-1365.
8. Condon, E.U and Shortley, G.H. (1935) *The Theory of Atomic Spectra*, Cambridge University Press, Cambridge.
9. Rotenberg, M., Bivens, R., Metropolis, N., and Wooten Jr., J.K. (1959) *The 3-j and 6-j Symbols*, M.I.T Press, Cambridge.
10. Runciman, W.A. (1956) Stark-splitting in crystals, *Phil. Mag.* **1**, 1075-1077.
11. Judd, B.R. (1962) Optical absorption intensities of rare-earth ions, *Phys. Rev.* **127**, 750-761.
12. Ofelt, G.S. (1962) Intensities of crystal spectra of rare-earth ions, *J. Chem. Phys.* **37**, 511-520.
13. Nielson, C.W. and Koster, G.F. (1963) *Spectroscopic coefficients of the p^n, d^n, and f^n configurations*, The M.I.T. Press, Cambridge.
14. Leavitt, R.P. and Morrison, C.A. (1980) Crystal-field analysis of triply ionized rare earth ions in lanthanum fluoride. II. Intensity calculations, *J. Chem. Phys.* **73**, 749-757.
15. Shortley, G.H. (1940) The computation of quadrupole and magnetic dipole transitions, *Phys. Rev.* **57**, 225-237.
16. Walsh, B.M., Barnes, N.P., and Di Bartolo, B. (1998) Branching ratios, cross sections, and radiative lifetimes of rare earth ions in solids: Application to Tm^{3+} and Ho^{3+} ions in $LiYF_4$, *J. Appl. Phys.* **83**, 2772-2787.
17. McCumber, D.E. (1964) Einstein relations connecting broadband emission and absorption spectra, *Phys. Rev.* **136**, A954-A957.
18. Payne, S.A., Chase, L.L., Smith, L.K., Kway, W.L., and Krupke, W.F. (1992) Infrared cross-section measurements for crystals doped with Er^{3+}, Tm^{3+}, and Ho^{3+}, *IEEE J. Quant. Elec.* **28**, 2619-2629.
19. Moulton, P.F. (1986) Spectroscopic and laser characteristics of Ti:Al_2O_3, *J. Opt. Soc. Am. B* **3**, 125-133.
20. Dunnina, E.B, Kaminskii, A.A., Kornienko, A.A., Kurbanov K., and Pukhov K.K. (1990) Dependence of line strength of electrical dipole f-f transitions on the multiplet energy of Pr^{3+} ion in $YAlO_3$, *Sov. Phys. Solid State* **32**, 920-922.
21. Quimby, R.S. and Miniscalco, W.J. (1994) Modified Judd-Ofelt technique and application to optical transitions in Pr^{3+}-doped glass, *J. Appl. Phys.* **75**, 613-615.
22. Goldner, P. and Auzel, F. (1996) Application of standard and modified Judd-Ofelt theories to a praseodymium fluorozirconate glass, *J. Appl. Phys.* **79**, 7972-7977.
23. Downer, M.C., Burdick, G.W., and Sardar, D.K. (1988) A new contribution to spin-forbidden rare-earth optical transition intensities: Gd^{3+} and Eu^{3+}, *J. Chem. Phys.* **89**, 1787-1797.
24. Burdick, G.W., Downer, M.C., and Sardar, D.K. (1989) A new contribution to spin-forbidden rare earth optical transition intensities: Analysis of all trivalent lanthanides, *J. Chem. Phys.* **91**, 1511-1520.
25. Tanaka, M., Nishimura, G., and Kushida, T. (1994) Contribution of J mixing to the $^5D_0$-$^7F_0$ transition of Eu^{3+} ions in several host matrices, *Phys. Rev. B* **49**, 16917-16925.
26. Tanaka, M. and Kushida, T. (1996) Interference between Judd-Ofelt and Wybourne-Downer mechanisms in the $^5D_0$-$^7F_0$ (J = 2,4) transitions of Sm^{3+} in solids, *Phys. Rev. B* **53**, 588-593.
27. Kushida, T. and Tanaka, M. (2002) Transition mechanisms and spectral shapes of the $^5D_0$-$^7F_0$ line of Eu^{3+} and Sm^{3+} in solids, *Phys. Rev. B* **65**, 195118(1-6).

28. Kushida, T., Kurita, A., and Tanaka, M. (2003) Spectral shape of the $^5D_0$-$^7F_0$ line of Eu^{3+} and Sm^{3+} in glass, *J. Lumin.* **102-103**, 301-306.
29. Lowther, J.E. (1974) Spectroscopic transition probabilities of rare earth ions, *J. Phys. C* **7**, 4393-4402.
30. Xia, S. and Chen, Y. (1985) Effect of J-mixing on the intensities of f-f transitions of rare earth ions, *J. Lumin.* **33**, 228-230.
31. Smentek, L. and Hess Jr., B.A. (1997) Theoretical description of 0↔0 and 0↔1 transitions in the Eu^{3+} ion in hosts with C_{2v} symmetry, *Mol. Phys.* **92**, 835-845.
32. Reid, M.F. and Richardson, F.S. (1983) Electric dipole intensity parameters for lanthanide 4f→4f transitions, *J. Chem. Phys.* **79**, 5735-5742.
33. Reid, M.F., Dallara, J.J., and Richardson, F.S. (1983) Comparison of calculated and experimental 4f→4f intensity parameters for lanthanide complexes with isotropic ligands, *J. Chem. Phys.* **79**, 5743-5751.
34. Malta, O.L. and Carlos, L.D. (2003) Intensities of 4f-4f transitions in glasses, *Quim. Nova* **26**, 889-895.
35. Wybourne, B.G. (1968) Effective operators and spectroscopic properties, *J. Chem. Phys.* **48**, 2596-2611.
36. Smentek, L. and Wybourne, B.G. (2000) Relativistic f↔f transitions in crystal fields, *J. Phys. B: At. Mol. Opt. Phys.* **33**, 3647-3651.
37. Smentek, L. and Wybourne, B.G. (2001) Relativistic f↔f transitions in crystal fields: II. Beyond the single-configuration approximation, *J. Phys. B: At. Mol. Opt. Phys.* **34**, 625-630.
38. Wybourne, B.G. and Smentek, L. (2002) Relativistic effects in lanthanides and actinides, *J. Alloys and Compounds* **341**, 71-75.
39. Peacock, R.D. (1975) The intensities of f↔f transitions, *Structure and Bonding* **22**, 83-122.
40. Smentek, L. (1998) Theoretical description of the spectroscopic properties or rare earth ions in crystals, *Physics Reports* **297**, 155--237.
41. Smentek, L. and Hess Jr., A. (2003) 40th Anniversary of the Judd-Ofelt Theory (special issue), *Mol. Phys.* **101** (7).
42. Kushida, T. (1972) Energy transfer and cooperative optical transitions in rare-earth doped inorganic materials: I. Transition probability calculation, *J. Phys. Soc. Japan* **34**, 1318-1326.
43. Kushida, T. (1972) Energy transfer and cooperative optical transitions in rare-earth doped inorganic materials: II. Comparison with experiment, *J. Phys. Soc. Japan* **34**, 1327-1333.
44. Kushida, T. (1972) Energy transfer and cooperative optical transitions in rare-earth doped inorganic materials: III. Dominant transfer mechanism, *J. Phys. Soc. Japan* **34**, 1334-1337.
45. Peacock, R.D. (1972) The sensitivity of computed Judd-Ofelt parameters to the particular transitions used, *Chem. Phys. Lett.* **16**, 590-592.
46. Peacock, R.D. (1971) Spectral intensities of the trivalent lanthanides. Part I. Solution spectra of heteropoly-complexes of Pr^{3+} and Ho^{3+}, *J. Chem. Soc.* (A), 2028-2031.
47. Peacock, R.D. (1972) Spectral intensities of the trivalent lanthanides. Part II. An assessment of the vibronic contribution, *J.C.S. Faraday II* **68**, 169-173.
48. Peacock, R.D. (1973) Spectral intensities of the trivalent lanthanides. Part III. The variation of the Judd-Ofelt parameters across an isostructural series, *Mol. Phys.* **25**, 817-823.
49. Jorgensen, C.K. and Reisfeld (1983) R. Judd-Ofelt parameters and chemical bonding *J. Less-Common Metals* **93**, 107-112.
50. Reisfeld, R. and Jorgensen, C.K. (1987) Excited state phenomena in vitreous materials, Chapter 58 *Handbook on the Physics and Chemistry of Rare Earths*, Elsevier Science Publishers B.V.
51. Edvardsson, S., Wolf, M., Thomas, J.O. (1992) Sensitivity of optical-absorption intensities for rare-earth ions, *Phys. Rev. B* **45** 10918-10923.
52. Wolf, M., Edvardsson, S., Zendejas, M.A., Thomas, J.O. (1993) Molecular-dynamics-based analysis of the absorption spectra of Nd^{3+}-doped Na^+ β″-alumina, *Phys. Rev. B* **48** 10129-10136.
53. Edvardsson, S., Ojamae, L., Thomas, J.O. (1994) A study of vibrational modes in Na^+ β -alumina by molecular dynamics simulation, *J. Phys. Condens. Matter* **6** 1319-1332.
54. Edvardsson, S., Klintenberg, M., Thomas, J.O. (1996) Use of polarized optical absorption to obtain structural information for Na^+/Nd^{3+} β″-alumina, *Phys. Rev. B* **54** 17476-17485.
55. Klintenberg, M., Edvardsson, S., Thomas, J.O. (1997) Calculation of energy levels and polarized oscillator strengths for Nd^{3+}:YAG, *Phys. Rev. B* **55** 10369-10375.